Heliyon

Received:
11 September 2018
Revised:
10 November 2018
Accepted:
6 December 2018

Cite as: Chen Klein, Doron Cohen-Elias, Gabby Sarusi. Controlling graphene work function by doping in a MOCVD reactor. Heliyon 4 (2018) e01030. doi: 10.1016/j.heliyon.2018.e01030

Controlling graphene work function by doping in a MOCVD reactor

Chen Klein [a], **Doron Cohen-Elias** [b], **Gabby Sarusi** [a,*]

[a] *Electrooptic and Photonics Engineering Department, Ben-Gurion University of the Negev and Ilse Katz Center for Nanoscience and Nanotechnology, Beer Sheva, 8410501, Israel*

[b] *Soreq NRC, The Israeli Center for Advanced Photonics, Yavne, Israel*

[*] Corresponding author.

E-mail address: sarusiga@bgu.ac.il (G. Sarusi).

Abstract

Here we demonstrate a new method for doping graphene using Metal Organic Chemical Vapor Deposition (MOCVD) reactor. The original undoped graphene was of a very high quality mounted on Si/SiO_2 substrates, they were then doped in the MOCVD's reactor using tertiarybutylphosphine (TBP) and tertiarybutylarsene (TBA). Post process Raman spectroscopy confirmed the presence of a single layer of phosphor doped graphene (G/P) and Arsine doped graphene (G/As) when doped by TBP or by TBA, respectively. Blue shift of the 2D peak assured p-type doping. The work function determined by ultraviolet photoelectron spectroscopy varied from 4.5 eV for Pristine Graphene to 4.7, 4.8 eV for G/As, G/P, respectively. The increase of the work function is attributed to electron transfer from the graphene to the dopant. Our results suggest that doping graphene by MOCVD with TBA or TBP can easily and effectively alternate the work function by few tenths of eV and improve the electronic properties of graphene. The MOCVD technology of doping graphene opens a new route on which other semiconductors can be epitaxially grown on it in a continues process in the same MOCVD reactor.

Keywords: Materials science, Nanotechnology

https://doi.org/10.1016/j.heliyon.2018.e01030

1. Introduction

Graphene is a basic structural element of many carbon allotropes such as carbon nanotubes, graphite and fullerenes [1]. It is one of the most promising nanomaterials due to its excellent electrical charge transport [2], thermal conductivity [3], and optical transparency [4].

The unique characteristics of graphene stem from its honeycomb lattice which consists of two equivalent sub-lattices of carbon atoms bonded by σ bonds. Although these σ bonds are within the 2D plane, the main bond that contributes to the delocalized network of electrons is the π bond, which is out of the plane bond [5]. Due to these unique characteristics of high lateral conductivity and optical transparency, graphene has attracted many researchers and engineering communities in making optoelectronic devices via graphene doping [6]. Many methods have been suggested to enhance the properties (electrical and optical) of graphene such as chemical doping [7], deposition of alkali metals [8] and substitutional doping [9]. Although these methods successfully enhance the properties of graphene, still they tend to damage the basal plane of graphene and eventually reduce its carrier's mobility [10]. On the other hand, there are methods, such as noncovalent and covalent doping that do not disturb graphene's structure and hence maintain it electron's high mobility. In those methods, the dopant ions are physically adsorbed on the surface of the graphene without modifying its structure. These methods minimally damage the basal plane of graphene and result in an enhancement of the electrical parameters [11]. Another parameter that should be taken into consideration when doping is variation of the work function due to doping. The work function of graphene can be varied by shifting the Fermi level due to of both, addition of electrons to the conduction band (n-doping) or removal of electrons from the valence band (p-doping) [12]. Changing the work function of electrode such as anode or a cathode can be used to reduce the potential barrier of organic devices such as: organic light emitting diodes (OLED). Therefore, variation of the work function in the graphene layer is crucial for improving device performances [13]. Researches have tried to control the work function of graphene by using different materials such as Au-ion, NH_3, self-assembled monolayer or metal oxide interlayer all these materials have shown P type doping which caused the work function to increase [13, 14, 15, 16, 17]. Chemical doping was also used a method to dope graphene and hence modulate the work function. Metals with high work function such as Au, Ir, Mo, Os, Pd, were used to increase the work function of graphene [18]. Such doping varied the Fermi level without introducing substitutional impurities, or damage to the basal plane, which can interrupt the conjugated network [19]. Researchers have been seeking for alternative source for doping graphene at a lower temperature, [20]. One of the possible dopants sources for phosphorus and arsenic doping are tertiarybutylphosphine (TBP) and tertiarybutylarsene

https://doi.org/10.1016/j.heliyon.2018.e01030

(TBA), respectively, which start to decompose at low temperature around 400^{O}C. Phosphorus has five valence electrons, but on the third electron shell, yielding a significantly larger covalent atomic radius of 106 pico-meter (pm), compare with 77 pm for Carbon, 82 pm for Boron and 75 pm for Nitrogen. Cruz-Silva et al. [21] used Density Functional simulations (DFT) to show that phosphorus can attach to carbon atoms; however they showed that this attachment can strongly modify the structural carbon lattice due to structural strain. Denis et al. [22] employed the first principle calculations to study the doping of graphene by phosphorus. Their results showed that phosphorus can open a large band gap (from 0.66 to 0.1 eV) and that it is possible to tune the band gap of graphene when doping with phosphorus. In another research, Dai et al. [23] used DFT calculations and found that adsorption of gas molecules can be strongly detected after doping Graphene with phosphorus. They should that by doping Graphene with phosphorus the electrical properties of Graphene can be varied, which can be used to detect toxic gases [23]. Substitutional doping of phosphorus on Cu was researched by Larrude et al. [24]. They found that doping Graphene with phosphorus increases the work function and that the doping mechanism in is attributed to electron transfer from the Graphene to the Cu substrate [24]. Arsenic, like phosphorus, has five valence electrons, it has a similar electronegativity and ionization energies to phosphorus and as such readily forms covalent molecules with most of the nonmetals. Its covalent atomic radius is higher than phosphorus (119 pm, compared with 106 pm). Denis et al. [25] investigated doped graphene by Arsenic using Density Functional Theory (DFT) and compared heteroatoms doping of graphene with Gallium, Germanium, Arsenic, and Selenium Atoms. They showed that doping Graphene with Arsenic offers a widest range of gap variation with respect to dopant concentration (from 0.3 to 1.3 eV).

In this paper, we report on doping of graphene in a MOCVD reactor using TBA as arsenic precursor and TBP as phosphorus precursor. Doping graphene by MOCVD has many advantages such as: ability to produce conformable coatings [26], a proven technology for large area deposition [27], ability to handle material with high vapor deposition [28], and capability to produce multilayer's [29]. The MOCVD technology of doping graphene opens a new route on which other semiconductors can be epitaxially grown on it in continues process in the same MOCVD reactor [30, 31]. We optimized the doping conditions through Raman spectroscopy, X-ray photoelectron spectroscopy (XPS), Ultra violet photoelectron spectroscopy (UPS), and electrical measurement analyses. Understanding the factors which govern the doping properties will open unique paths for controlling the physical properties of graphene, thus allowing the tailoring of materials for designated devices and applications.

https://doi.org/10.1016/j.heliyon.2018.e01030

2. Experimental

Monolayer graphene was grown by Chemical Vapor deposition (CVD) on copper catalyst (6×4 cm^2) and transferred to a Si/SiO_2 (2.5×2.5 cm^2) substrate using wet transfer process. Such ready samples can be purchased from companies such as "ACS materials", where the sheet resistance of the specimen is 450Ω/Sq^{-1}. The exposure to TBP in the MOCVD reactor was carried out using 3×2 inch Thomas Swan MOCVD system at pressure of 400Torr where the TBP flow was 70 sccm. During the doping the temperature was ramped to 650 °C (nominally) within 5 minutes, held for 5 minutes and cooled down naturally to 200 °C. The TBP was flowing through the reactor during the all these stages, where under 200 °C the TBP flow was terminated. The same procedure was performed for TBA accepts that during the doping the temperature was ramped to at 450 °C or 700 °C for 5 minutes, respectively.

3. Instrumentation

The quality of the graphene was evaluated by Raman spectroscopy using a confocal micro-Raman spectrometer (NT-MDT, NTEGRA SPECTRA) equipped with a 514 nm laser excitation source (power at sample is below 0.1 mW), a 100 objective and a CCD detector. The focused laser spot has a diameter of about 1−2μm, and the spectral resolution is about 3 cm^{-1}. The wavenumber calibration was achieved based on the standard values for crystalline silicon band checked at 520 cm^{-1} and the vibrational stretching mode of atmospheric nitrogen at 2332 cm^{-1}. All the spectra were recorded at room temperature. X-ray Photoelectron Spectroscopy (XPS) spectra were carried out in a UHV ESCALAB 290Xi spectrometer, equipped with a hemispherical electron energy analyzer. Kratos AXIS ULTRA system using a concentric hemispherical analyzer for photo-excited electron detection. XPS measurements were performed using a monochromatic Al Kα X-ray source ($h\nu = 1486.6$ eV) at 75W and detection pass energies ranging between 20 and 80 eV. UPS measurements were carried out with Kratos AXIS ULTRA system using a concentric hemispherical analyzer for photo-excited electron detection. UPS was measured with helium discharge lamp, using He I (21.22 eV) and He II (40.8 eV) radiation lines. Energy scale was referenced to the Fermi level measured on bare Au substrate. The vacuum level was obtained from the secondary-electron cutoff (photoemission onset) measured in the low kinetic energy region of the He (I) spectra. Total energy resolution was less than 100 meV, as was determined from the Fermi edge of Au reference sample. Hall Effect measurements were performed to obtain the charge carriers' type, density and mobility. In the Hall measurements, the magnetic fields varied from 0 KG and 10 KG The field step was 1 KG. For electrical measurements (Hall effect and sheet conductivity) Indium electrodes were placed according the

https://doi.org/10.1016/j.heliyon.2018.e01030

van der Paw geometry to determine the four-probe conductivity, σ_S (from the sheet resistance, R_S) of the sample at every stage of the measurement.

4. Results and discussion

Raman of Pristine Graphene is characterized by 3 main peaks, the 2D peak (3100 cm^{-1}), G peak (1580 cm^{-1}), and D peak (1360 cm^{-1}). The 2D peak originates from a second-order Raman scattering process in which two phonons are created [32]. The G peak originates from the doubly-degenerate in-plane sp^2 carbon atoms stretching mode [32]. The D peak originates from the second-order Raman scattering processes in which two phonons with equal and opposite wavevector are created [32]. The 2D peak is mostly used for distinguishing between a single layer Graphene and a multilayer Graphene [25]. The D peak is widely used to denote defects in the Graphene sample [32]. Raman spectrum of undoped graphene ($Si/SiO_2/G$) is clearly different from doped graphene by As ($Si/SiO_2/G/As$) at 450 °C and 700 °C respectively Fig. 1 (A,B). The G peak position of graphene is blue-shifted from 1580 to 1597, 1601 cm^{-1} for 450 °C and 700 °C, respectively, as shown in Fig. 1 (A,B). Variation of the 2D peak position can also be observed, indicating the increasing

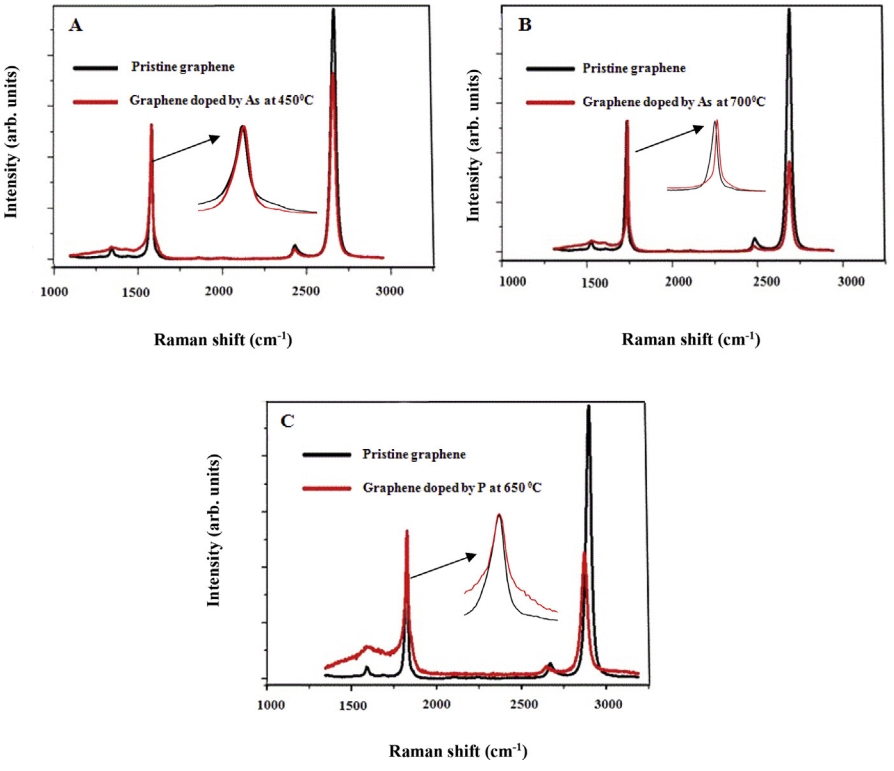

Fig. 1. Raman spectra of $Si/SiO_2/G$ (black) graphene doped with $Si/SiO_2/G/As$ (red) at 450 °C (A) and 700 °C (red) (B) respectively, and $Si/SiO_2/G$ (black)and $Si/S\ SiO_2/G/P$ at 650 °C (red) (C).

https://doi.org/10.1016/j.heliyon.2018.e01030

doping concentrations. Noticeably, the I_{2D}/I_G ratio, that is used to estimate the doping intensity, decreases after increasing of the temperatures. The ratio is reduced from 1.9 for pristine graphene to 1.4 and 0.8, for 450 °C and 700^{0}C-doped graphene, respectively. The Raman spectrum features of the changing peak positions and the I_{2D}/I_G ratio confirms the doping increases with temperature. The Raman spectrum also shows a variation in the D peak, indicating a higher defect density of the basal plane. Raman spectra of un-doped ($Si/SiO_2/G$) and graphene doped by P ($Si/SiO_2/G/P$) at different temperatures are shown in Fig. 1(C). The G (1588 cm^{-1}) and 2D (3086 cm^{-1}) peaks are shifted by 11 cm^{-1} and 19 cm^{-1}, respectively. The Raman spectrum of $Si/SiO_2/G/P$ also shows a change in D peak, which also indicates of the existence of a high defect density of the basal plane. Variation of the 2D peak position is also observed, which indicates an increase due to doping concentrations [33].

Fig. 2 shows XPS spectra of un-doped and the P and As doped graphene layers on Si/S SiO_2 substrate. The quantitative chemical analysis of each graphene film, obtained from these spectra, is summarized in Table 1. The As and P atomic % values reported in Table 1 are relative to the carbon content.

In all tested samples, as expected, carbon signal is well observed (Table 1) indicating presence of graphene indicating that graphene layer was not removed or destroyed during the doping process. Presence of small amount of P signal (Fig.2 C, D) in the doped sample ($Si/SiO_2/G/P$) reveals a small amount of doping which can be seen in Table 1.

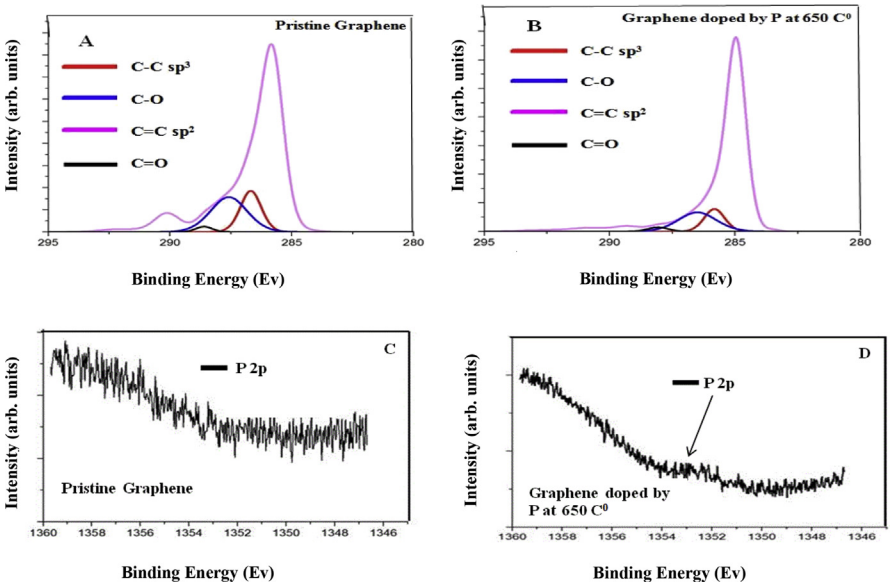

Fig. 2. High resolution C1s XPS spectra of $Si/SiO_2/G$ (a) and $Si/SiO_2/G/P$ (b) films. The three features C═C sp^2, C−C sp^3, C−O and C═O are also shown. High resolution XP spectra of the P_{2p} (c, d) regions for $Si/SiO_2/G$ (A, B), undoped and doped Graphene with P (C, D) samples.

https://doi.org/10.1016/j.heliyon.2018.e01030

Table 1. Elemental composition of $Si/SiO_2/G$, Graphene doped with $Si/SiO_2/G/P$ and Graphene doped with $Si/SiO_2/G/As$ at different temperatures.

	O	C	As	P
Undoped Graphene	38.9	41.5	-	-
Graphene Doped by As 450 °C	45.8	37.4	0.08	-
Graphene Doped by As 700 °C	47.5	30.5	0.12	-
Graphene Doped by P 650 °C	46.8	32.1	-	0.06

As can be seen in Fig. 3, in As doped graphene samples ($Si/SiO_2/G/As$) doped at 450 °C and 700 °C (Fig 3 A,B), As signal is observed, indicating successful doping process (Fig. 3 C,D).

Three main peaks in the XPS spectra can be seen (Figs. 2(A,B), 3 (A,B)). The peak at 285.3 eV is related to C═C sp^2 bonds, another one at 285.5 eV is related to C−C sp^3, another one at 286.2 eV which is related to C−O bonds, and the last one at 288.8 eV is related to C═O bonds. Kwon et al. [34] found out that when doping graphene with different metal chlorides; the C1s core level can be affected due to the doping process. This affect is shown in the XPS (Figs. 2(A,B), 3 (A,B)) throw variation in the $I_{C=C}/I_{C-C}$ intensity ratio. For all doped samples (with P, and As) the $I_{C=C}/I_{C-C}$ intensity ratio increases. These results are correlated with Kwon et al. [34], which showed that increased $I_{C=C}/I_{C-C}$

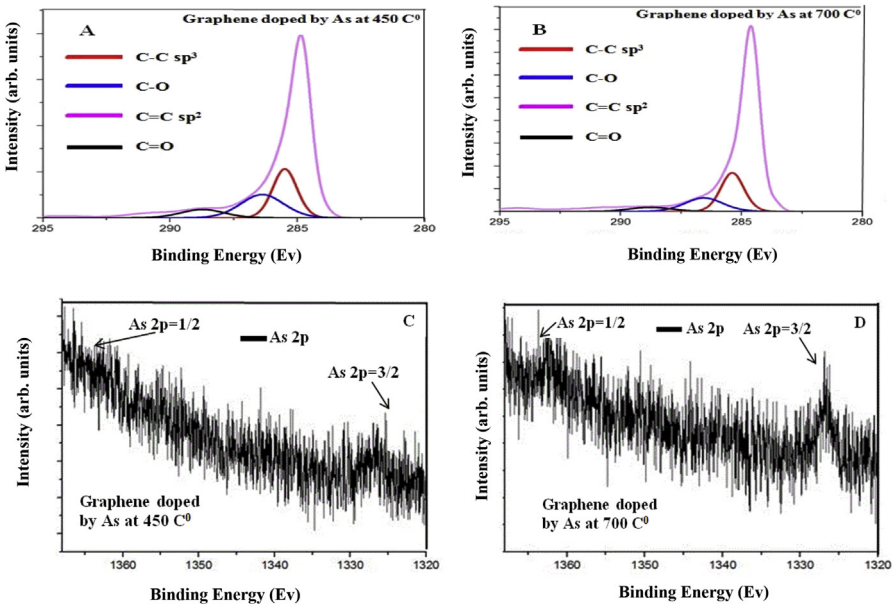

Fig. 3. High resolution C1s XPS spectra of $Si/SiO_2/G/As$ at 450 °C (A) and $Si/SiO_2/G/As$ at 700 °C (B) films. The three features C═C sp^2, C−C sp^3 C−O and C═O are also shown. High resolution XP spectra of the P_{2p} (C−D) regions for Graphene doped with As (C, D) samples are also shown.

https://doi.org/10.1016/j.heliyon.2018.e01030

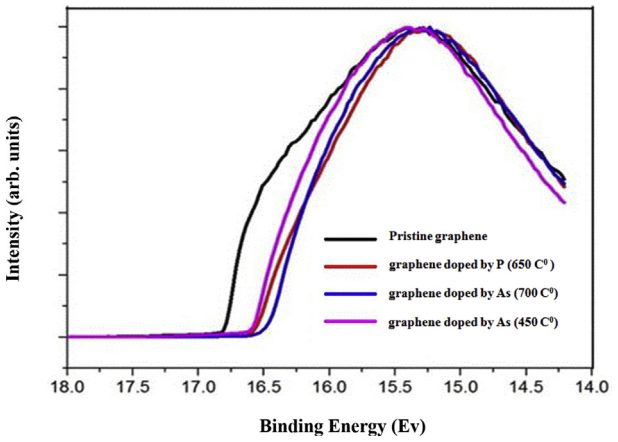

Fig. 4. UPS spectra covering the secondary electron threshold Region for $Si/SiO_2/G$ (black) $Si/SiO_2/G/As$ (purple (450 °C), blue (700 °C)) and $Si/SiO_2/G/P$ (red) (650 °C) at different temperatures.

intensity ratio can be associated with p-doping. The C−O percentage is also reduced in the doped graphene (P, and As).In C═O the variation due to doping was non-significant. This result, together with the increase of the oxygen atomic % during the doping procedure (see Table 1) can affect the electrical properties of the graphene (sheet resistance, mobility etc.).

To investigate the influence of doping Graphene with P and As the work function (WF) was measured by ultraviolet photoemission spectra (UPS) (Fig. 4). The cutoff binding energies (E_{cutoff}) determined by the extrapolation procedure and the work function obtained by subtraction of $\Phi = 21.2$ by E_{cutoff} is shown. The effect of As and P doped graphene on the work function was analyzed by UPS. Fig. 4 shows the secondary electron cutoff region of the $Si/SiO_2/G$, $Si/SiO_2/G/As$ and $Si/SiO_2/G/P$ at different temperatures.

The secondary electron cutoff was determined by extrapolating two dashed lines from the background and the onset in the secondary electron threshold. The work function of the Si/S iO_2/G was measured to be 4.5 eV, which is close to values reported in the literature [35/27]. The work function value obtained for $Si/SiO_2/G/As$ at 700 °C was 4.8 eV and for $Si/SiO_2/G/As$ at 450 °C was 4.67 eV. The work function value obtained for $Si/SiO_2/G/P$ was 4.7 eV. For all doped samples the work function increased. This behavior is typical for p-doped graphene, where the increase in the work function can be attributed to electron transfer, shifting the Fermi level from the Dirac point to the valence band. In order to understand the effect of P and As doped graphene on the sheet resistance and the mobility, the electrical properties of the doped graphene were measured. Fig. 5 shows the sheet resistance (A), and electron mobility (B), of annealed- pristine graphene (at 650 °C) (red), P-doped (at 650 °C) (brown), As-doped (700 °C) (orange), As-doped (450 °C) (blue)and As doped (at 650 °C) and measured at 77 K (green).

https://doi.org/10.1016/j.heliyon.2018.e01030

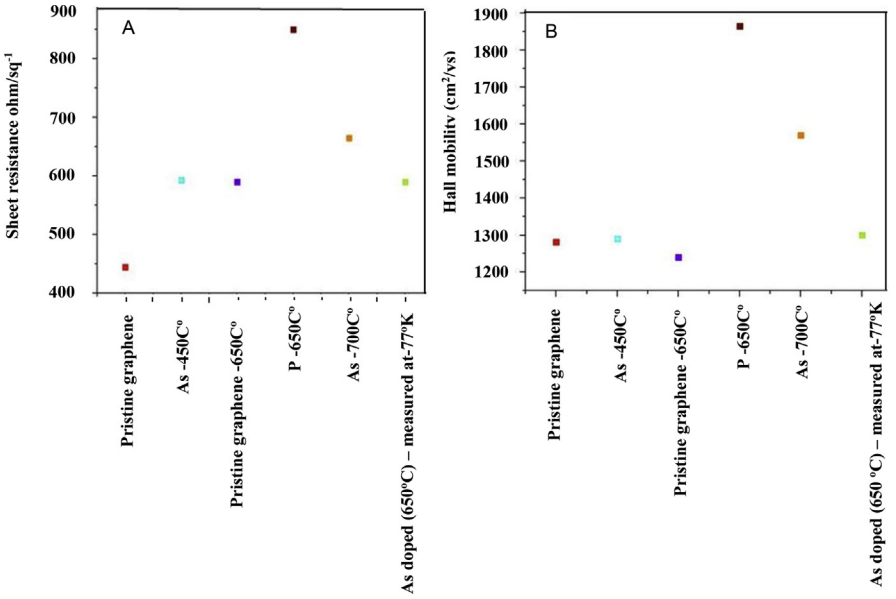

Fig. 5. Sheet resistance (A), electron mobility (B) of pristine graphene (red), annealed-un doped pristine graphene (650 °C) (purple), P-doped (650 °C) (brown), As-doped (450 °C) (blue), As-doped (700 °C) (orange) and As doped (650 °C) and measured at 77 °K (green).

The sheet resistance of pristine graphene and doped graphene were measured on Si/SiO_2 substrates and are presented in Fig. 5(A). The sheet resistance of pristine graphene gradually increases from 450 ohm/sq^{-1} to 593 ohm/sq^{-1}, 590 ohm/sq^{-1}, 665 ohm/sq^{-1} and 850 ohm/sq^{-1} for pristine graphene, annealed-pristine graphene doped at 650 °C, As-doped graphene at 450 °C, As-doped graphene at (700 °C) and P doped (650 °C), respectively. The sheet resistance increases could be attributed to the formation of lattice defects formation, which are caused during doping at high temperatures, this can be seen on the Raman analysis (Fig 1 A–C) that the 2D peak and the D peaks varies. Hall measurement provides the doping type as well; the results obtained matched that of the UPS measurements which showed P type doping. The mobility of each sample was calculated (Fig. 5B) from Hall measurements. The estimated mobility of pristine graphene was 1290 cm^2 V^{-1} s^{-1}. After annealing (at 650 °C) for 5 min it was found out that there was no change in the mobility. Doping graphene with As at 450 °C for the same duration, showed slightly decrease in electron mobility to 1250 cm^2/V^{-1} s^{-1}. On the other hand, when increasing the annealing temperature to 700 °C the mobility increased to 1570cm^2 V^{-1} s^{-1}. When doping with P the mobility increased as high as 1865 cm^2/V^{-1} s^{-1}. Carrier concentrations of annealed-pristine graphene at 650 °C was 8×10^{12} cm^{-2}, and for As-doped graphene at 450 °C, As-doped graphene at (700 °C) and P doped (650 °C), was 8×10^{12}, 6×10^{12} cm^{-2}, 4×10^{12} cm^{-2} respectively. So no significant variation can be seen due to the doping process. Our results show that when temperature increases, formation of clusters (P,As) may take place.

https://doi.org/10.1016/j.heliyon.2018.e01030

This cluster formation can be attributed to increase in thermal energy. This may lead to an enhancement in mobility and reduction in graphene doping level. Theoretical models [36, 37] have shown that cluster formation is attributed to increase in mobility. Our results are consistent with these models and emphasis the critical role of low level doping in Graphene [38].

5. Conclusion

In summary, we have investigated the effect of As and P doping on graphene when done in a MOCVD reactor. After doping, Raman results showed a blue shift of the G band in $Si/SiO_2/G/P$, and $Si/SiO_2/G/As$, which indicates p-type doping. The increase in the work function from 4.5 eV in $Si/SiO_2/G$ to 4.7 eV in $Si/SiO_2/G/P$, and to 4.8 eV in $Si/SiO_2/G/As$ suggests also p type-doped graphene which agrees with the Raman measurements. The doping mechanism in $Si/SiO_2/G/P$, and in $Si/SiO_2/G/As$ can clearly indicate electrons are transferred from the doped graphene to the dopant (As,P). The electrical properties of pristine graphene, and on doped graphene; $Si/SiO_2/G/P$ and $Si/SiO_2/G/As$, were measured by Hall effect and sheet resistance in order to investigate the doping effect on these properties. The results showed that after doping, there is an increase in the mobility. Our results show that doping graphene by MOCVD with TBA or TBP can easily and effectively vary the electronic properties of graphene.

Declarations

Author contribution statement

Chen Klain: Conceived and designed the experiments; Performed the experiments; Analyzed and interpreted the data; Wrote the paper.

Doron Cohen-Elias: Performed the experiments; Analyzed and interpreted the data; Contributed reagents, materials, analysis tools or data.

Gabby Sarusi: Conceived and designed the experiments; Analyzed and interpreted the data; Contributed reagents, materials, analysis tools or data; Wrote the paper.

Funding statement

This research did not receive any specific grant from funding agencies in the public, commercial, or not-for-profit sectors.

Competing interest statement

The authors declare no conflict of interest.

https://doi.org/10.1016/j.heliyon.2018.e01030

Additional information

No additional information is available for this paper.

References

[1] Hideo Aoki, Mildred S. Dresselhaus, Physics of Graphene, second ed., Springer, 2013.

[2] K.S. Novoselov, A.K. Geim, S.V. Morozov, D. Jiang, M.I. Katsnelson, I.V. Grigorieva, S.V. Dubonos, A.A. Firsov, Two-dimensional gas of massless Dirac fermions in graphene, Nature 438 (2005) 197−200.

[3] A.A. Balandin, S. Ghosh, W. Bao, I. Calizo, D. Teweldebrhan, F. Miao, C.N. Lau, 10. Superior Thermal Conductivity of Single-layer Graphene.pdf, 2008.

[4] K.S. Novoselov, D. Jiang, F. Schedin, T.J. Booth, V.V. Khotkevich, S.V. Morozov, A.K. Geim, Two-dimensional atomic crystals, Proc. Natl. Acad. Sci. Unit. States Am. 102 (2005) 10451−10453.

[5] A.K. Geim, K.S. Novoselov, The rise of graphene, Nat. Mater. 6 (2007) 183−191.

[6] Qingbin Zheng, Jang-Kyo Kim, Graphene for Transparent Conductors Synthesis, Properties and Applications, first ed., Springer, 2015.

[7] H. Liu, Y. Liu, D. Zhu, Chemical doping of graphene, J. Mater. Chem. 21 (2011) 3335−3345.

[8] J.H. Chen, C. Jang, S. Adam, M.S. Fuhrer, E.D. Williams, M. Ishigami, Charged-impurity scattering in graphene, Nat. Phys. 4 (2008) 377−381.

[9] L.S. Panchakarla, K.S. Subrahmanyam, S.K. Saha, A. Govindaraj, H.R. Krishnamurthy, U.V. Waghmare, C.N.R. Rao, Synthesis, structure, and properties of boron- and nitrogen-doped graphene, Adv. Mater. 21 (2009) 4726−4730.

[10] D. Wei, Y. Liu, Y. Wang, H. Zhang, L. Huang, G. Yu, Synthesis of N-doped graphene by chemical vapor deposition and its electrical properties, Nano 9 (2009) 1752−1758.

[11] H. Pinto, A. Markevich, Electronic and electrochemical doping of graphene by surface adsorbates, Beilstein J. Nanotechnol. 5 (2014) 1842−1848.

[12] S.A. Paniagua, J. Baltazar, H. Sojoudi, S.K. Mohapatra, S. Zhang, C.L. Henderson, S. Graham, S. Barlow, S.R. Marder, Production of heavily

https://doi.org/10.1016/j.heliyon.2018.e01030

n- and p-doped CVD graphene with solution-processed redox-active metal-organic species, Mater. Horizons. 1 (2014) 111−115.

[13] H.-J. Shin, W.M. Choi, D. Choi, G.H. Han, S.-M. Yoon, H.-K. Park, S.-W. Kim, Y.W. Jin, S.Y. Lee, J.M. Kim, J.-Y. Choi, Y.H. Lee, Control of electronic structure of graphene by various dopants and their effects on a nanogenerator, J. Am. Chem. Soc. 132 (2010) 15603.

[14] A. Benayad, H.-J. Shin, H.K. Park, S.-M. Yoon, K.K. Kim, M.H. Jin, H.-K. Jeong, J.C. Lee, J.-Y. Choi, Y.H. Lee, Au nanoparticle-decorated graphene electrodes for GaN-based optoelectronic devices, Chem. Phys. Lett. 475 (2009) 91.

[15] D. Wei, Y. Liu, Y. Wang, H. Zhang, L. Huang, G. Yu, Synthesis of N-doped graphene by chemical vapor deposition and its electrical properties, Nano Lett. 9 (2009) 1752.

[16] Y. Shi, K.K. Kim, A. Reina, M. Hofmann, L.-J. Li, J. Kong, Work function engineering of graphene electrode via chemical doping, ACS Nano 4 (2010) 2689.

[17] J. Park, W.H. Lee, S. Huh, S.H. Sim, S.B. Kim, K. Cho, B.H. Hong, K.S. Kim, Work-function engineering of graphene electrodes by self-assembled monolayers for high-performance organic field-effect transistors, J. Phys. Chem. Lett. 2 (2011) 841.

[18] Y. Wang, S.W. Tong, X.F. Xu, B. Özyilmaz, K.P. Loh, Interface engineering of layer-by-layer stacked graphene anodes for high-performance organic solar cells, Adv. Mater. 23 (2011) 1514.

[19] D.R. Lide, CRC Handbook on Chemistry and Physics, CRC Press LLC, Cleveland, OH, 2008, pp. 12−114.

[20] J. Zhang, J. Li, Z. Wang, X. Wang, W. Feng, W. Zheng, W. Cao, P. Hu, Low-temperature growth of large-area heteroatom-doped graphene film, Chem. Mater. 26 (2014) 2460−2466.

[21] E. Cruz-Silva, F. Lopez-Urias, E. Munoz-Sandoval, B.G. Sumpter, H. Terrones, J.C. Charlier, V. Meunier, M. Terrones, Phosphorus and phosphorus-nitrogen doped carbon nanotubes for ultrasensitive and selective molecular detection, Nanoscale 3 (2011) 1008−1013.

[22] P.A. Denis, Band gap opening of monolayer and bilayer graphene doped with aluminium, silicon, phosphorus, and sulfur, Chem. Phys. Lett. 492 (2010) 251−257.

[23] J. Dai, J. Yuan, Modulating the electronic and magnetic structures of P-doped graphene by molecule doping, J. Phys. Condens. Matter 22 (2010).

 https://doi.org/10.1016/j.heliyon.2018.e01030

[24] D.G. Larrude, Y. Garcia-Basabe, F.L. Freire Junior, M.L.M. Rocco, Electronic structure and ultrafast charge transfer dynamics of phosphorous doped graphene layers on a copper substrate: a combined spectroscopic study, RSC Adv. 5 (2015) 74189−74197.

[25] P.A. Denis, Chemical reactivity and band-gap opening of graphene doped with gallium, germanium, arsenic, and selenium atoms, ChemPhysChem 15 (2014) 3994−4000.

[26] G. Strauch, H. Juergensen, Deposition of ElectroceramicThin films by MOCVD, Adv. Mater. Opt. Electron. 167 (2000) 163−167.

[27] M. Deschler, E. Woelk, D. Schmitz, G. Strauch, H. Jürgensen, Multiwafer MOCVD systems for ferroelectrics, Integrated Ferroelectrics Int. J. 18 (1997) 119−125.

[28] M.J. Crosbie, P.A. Lane, P.J. Wright, D.J. Williams, A.C. Jones, T.J. Leedham, C.L. Reeves, J. Jones, Liquid injection metal organic chemical vapour deposition of lead−scandium−tantalate thin−lms for infrared devices, J. Cryst. Growth 219 (2000) 390−396.

[29] J. Lindner, F. Weiss, J.P. Senateur, W. Haessler, G. Kobernik, S. Oswald, A. Figueras, J. Santiso, Growth of BaTiO3/SrTiO3 superlattices by injection MOCVD, Integrated Ferroelectrics Int. J. 30 (2000) 53−59.

[30] N. Nepal, V.D. Wheeler, T.J. Anderson, F.J. Kub, M.A. Mastro, R.L. Myers-Ward, S.B. Qadri, J.A. Freitas, S.C. Hernandez, L.O. Nyakiti, S.G. Walton, K. Gaskill, C.R. Eddy, Epitaxial growth of III-nitride/graphene heterostructures for electronic devices, Appl. Phys. Express. 6 (2013).

[31] T. Li, C. Liu, Z. Zhang, B. Yu, H. Dong, W. Jia, Z. Jia, C. Yu, L. Gan, GaN epitaxial layers grown on multilayer graphene by MOCVD, AIP Adv. 8 (2018) 0451051−0451056.

[32] A.C. Ferrari, Raman spectroscopy of graphene and graphite: disorder, electron-phonon coupling, doping and nonadiabatic effects, Solid State Commun. 143 (2007) 47−57.

[33] A. Das, et al., Monitoring dopants by Raman scattering in an electrochemically top-gated graphene transistor, Nat. Nanotech. 3 (2008) 210−215.

[34] K.C. Kwon, K.S. Choi, S.Y. Kim, Increased work function in few-layer graphene sheets via metal chloride doping, Adv. Funct. Mater. 22 (2012) 4724−4731.

 https://doi.org/10.1016/j.heliyon.2018.e01030

[35] A. Siokou, F. Ravani, S. Karakalos, O. Frank, M. Kalbac, C. Galiotis, Surface refinement and electronic properties of graphene layers grown on copper substrate: an XPS, UPS and EELS study, Appl. Surf. Sci. 257 (2011) 9785−9790.

[36] M.I. Katsnelson, A.K. Geim, Electron scattering on microscopic corrugations in graphene, Philos. Trans. R. Soc. A Math. Phys. Eng. Sci. 366 (2008) 195−204.

[37] K.S. Novoselov, A.K. Geim, S.V. Morozov, Y.Z.D. Jiang, S.V. Dubonos, I.V. Grigorieva, A.A. Firsov, Electric field effect in atomically thin carbon films, Science (80-.) 306 (2004) 666−669.

[38] M.I. Katsnelson, K.S. Novoselov, Graphene: new bridge between condensed matter physics and quantum electrodynamics, Solid State Commun. 143 (2007) 3−13.